Letter

Polymer diffusive instability leading to elastic turbulence in plane Couette flow

Miguel Beneitez [1], Jacob Page [2], and Rich R. Kerswell [1]
[1] *DAMTP, Centre for Mathematical Sciences, Wilberforce Road, Cambridge CB3 0WA, United Kingdom*
[2] *School of Mathematics, University of Edinburgh, EH9 3FD, United Kingdom*

(Received 12 May 2023; accepted 7 August 2023; published 13 October 2023)

Elastic turbulence is a chaotic flow state observed in dilute polymer solutions in the absence of inertia. It was discovered experimentally in circular geometries and has long been thought to require a finite amplitude perturbation in parallel flows. Here we demonstrate, within the commonly used Oldroyd-B and FENE-P models, that a self-sustaining chaotic state can be initiated via a linear instability in a simple inertia-less shear flow caused by the presence of small but nonzero diffusivity of the polymer stress. Numerical simulations show that the instability leads to a three-dimensional self-sustaining chaotic state, which we believe is the first reported in a wall-bounded, parallel, inertia-less viscoelastic flow.

DOI: 10.1103/PhysRevFluids.8.L101901

Dilute polymer solutions are ubiquitous in everyday life (e.g., foods, shampoo, paints, cosmetics) and understanding how they behave is important for many industrial processes (e.g., plastics, oil, pharmaceuticals, and chemicals). The stretching and subsequent relaxation of the polymers introduces new viscoelastic stresses in the flow which depend on the flow's deformation history. As a result, polymer flows can exhibit startlingly different behavior from that of a Newtonian fluid like water (e.g., rod-climbing, die swell, and elastic recoil [1]). Perhaps most strikingly, a chaotic flow state—so-called "elastic turbulence" (ET)—can occur for vanishing inertia, in stark contrast to Newtonian fluid mechanics where inertia provides the only nonlinearity. ET has important applications in small-scale flows where, for example, enhanced mixing for chemical reactions or heat transfer for cooling computer chips are highly desirable [2,3]. Even though the origin of this behavior is still not understood, the key ingredients are believed to be fluid elasticity provided by the polymers and streamline curvature, which together give rise to a new elastic linear instability [4–7]. Experiments in curved geometries confirm the linear instability leads to sustained ET [8]. In contrast, wall-bounded inertia-less parallel polymer flow has been presumed linearly stable, and experimental work therefore has focused on triggering a finite amplitude instability instead. Obstacles in the flow have been used to provide the required streamline curvature believed necessary for this elastic instability and ultimately ET [9–12]. However, the requirements for both initiating such a transition and for the existence of a self-sustaining chaotic state in a planar geometry are unknown.

Recently, by exploring the large relaxation-time limit of the polymers, a new elastic linear instability was identified for the parallel flow of an Oldroyd-B fluid in a pipe or channel at finite inertia [13,14] and at vanishing inertia in a channel only [15]. This instability is a "center mode"—concentrated around the centerline of the channel—and is strongly subcritical, giving

rise to an arrowhead-shaped traveling wave solution [16] over a large region of the parameter space. This solution has been seen in simulations at both finite [17] and vanishing inertia [18,19], and may play a role in two-dimensional elastoinertial turbulence where inertia is important [20]. While no link has yet been found between this structure and ET in wall-bounded flows, similar arrowhead-like flow structures have been observed in doubly periodic "Kolmogorov flow" [21,22] where a self-sustaining, two-dimensional chaotic state is maintained in the absence of inertia. The chaotic dynamics found here can be directly connected to a linear instability of the basic state [23,24], though whether this instability is driven by the same mechanism as the center mode, or whether the nonlinear chaotic state is a manifestation of the three-dimensional ET found in wall-bounded flows is an open problem. In contrast to these configurations, the simpler case of constant shear between two differentially moving, parallel plates, known as plane Couette flow, has been considered linearly stable for all inertia and elasticity parameters [13].

In this Letter we report that viscoelastic plane Couette flow is linearly unstable if polymer stress diffusion is included in the model. This diffusion is generally so small that it is ignored as an important physical effect, but is reintroduced as a much larger "artificial" diffusion to stabilize time-stepping schemes if their inherent numerical diffusion is not sufficient. This diffusion-induced linear instability is distinctly different from the center-mode present in channels, being concentrated instead at the walls. Significantly, there is no smallest diffusion threshold below which the instability vanishes: the wavelength of the instability decreases with the size of the diffusion so the instability could be misunderstood as a numerical instability. The growth rate of the instability tends to a nonzero limit as the polymer diffusion goes to zero so the vanishing-diffusion limit is singular. The new diffusive instability exists over a very wide area of the parameter space and is robust to the choice of boundary conditions on the polymer conformation. Direct numerical simulations (DNS) show that the instability saturates onto a low-amplitude limit cycle in two dimensions. Three-dimensional simulations show a transition to sustained spatiotemporal chaos, which we believe to be the first reported computation of such a state in a planar geometry.

We consider the inertia-less flow of an incompressible, viscoelastic fluid between infinite plates at $y = \pm h$ moving with velocity $\pm U_0\hat{\mathbf{x}}$. The governing equations are

$$\nabla p = \beta\Delta\mathbf{u} + (1-\beta)\nabla\cdot\mathbf{T}(\mathbf{C}), \tag{1a}$$

$$\nabla\cdot\mathbf{u} = 0, \tag{1b}$$

$$\partial_t\mathbf{C} + (\mathbf{u}\cdot\nabla)\mathbf{C} + \mathbf{T}(\mathbf{C}) = \mathbf{C}\cdot\nabla\mathbf{u} + (\nabla\mathbf{u})^T\cdot\mathbf{C} + \varepsilon\Delta\mathbf{C}, \tag{1c}$$

where the polymeric stress $\mathbf{T}$ is related to the conformation tensor $\mathbf{C}$ using the FENE-P model

$$\mathbf{T}(\mathbf{C}) := \frac{1}{Wi}\left[\frac{\mathbf{C}}{1-(\mathrm{tr}\,\mathbf{C}-3)/L_{\max}^2} - \mathbf{I}\right].$$

This model successfully predicted the phenomenon of elastoinertial turbulence (EIT) in 2010 [25], which was observed a year later in experiments [26,27].

The equations are non-dimensionalized by half the gap width h and the plate speed U_0, which define the Weissenberg number $\mathrm{Wi} := \lambda U_0/h$ (the ratio of the polymer relaxation time λ to a flow timescale). The parameter $\beta := \mu_s/\mu_T$ is the ratio of the solvent-to-total viscosities while $\varepsilon := D/U_0h$ is the nondimensionalization of the polymer diffusivity D [28]. In this configuration, the laminar basic state is simply $\mathbf{U} = y\hat{\mathbf{x}}$ with only $T_{xx} = 2\mathrm{Wi}$ and $T_{xy} = 1$ being the nonzero stress components for an Oldroyd-B fluid ($L_{\max}\to\infty$). The polymer equation (1c) changes character from hyperbolic at $\varepsilon = 0$ to parabolic for $\varepsilon \neq 0$ and extra boundary conditions are then needed. Three boundary conditions are considered: (i) application of the governing equations with $\varepsilon = 0$ at the walls [29]; (ii) application of the governing equations with only the term $\varepsilon\partial_y^2 C_{ij}$ removed [17]; and (iii) Neumann, so $\partial_y C_{ij} = 0$.

The linear stability of the basic state is examined by introducing small perturbations of the form $\phi'(\mathbf{x},t) = \hat{\phi}(y)\exp[ik_x(x-ct)] + \mathrm{c.c.}$, where $k_x \in \mathbb{R}$ is the streamwise wave number and $c = c_r + ic_i$ a complex wavespeed, with instability if $c_i > 0$. The linear eigenvalue problem is

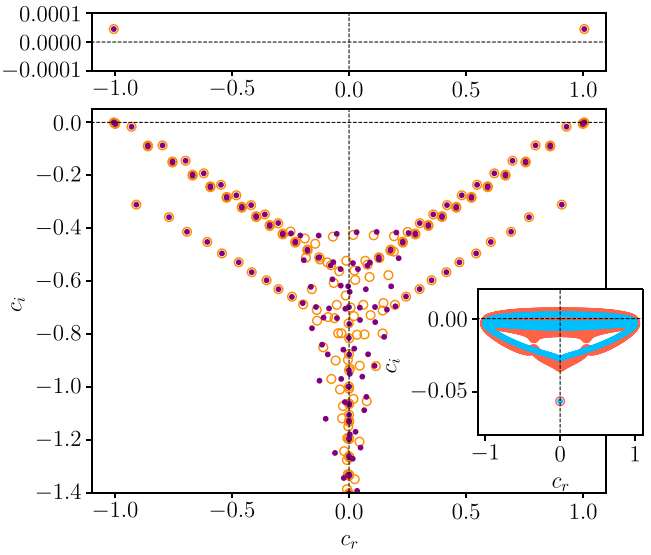

FIG. 1. Spectrum at Re = 0, Wi = 100, $\beta = 0.95$, $k_x = 3$ for two different resolutions $N_y = 300$ (orange circles) and $N_y = 400$ (purple dots) with $\varepsilon = 10^{-3}$ within the domain and $\varepsilon = 0$ at the boundaries. Top inset: Zoom-in to the unstable eigenvalues $c_i > 0$. Bottom right inset: Spectrum for the same parameters but $\varepsilon = 0$ everywhere in the domain and boundaries and two different resolutions $N_y = 300$ (red circles) and $N_y = 400$ (blue dots). The most unstable eigenvalues with finite ε here are $c = \pm 1.0052607137 + 4.513293285i \times 10^{-5}$ Note the apparent instabilities in the continuous spectrum seen in the $\varepsilon = 0$ results are associated with poor resolution of the (nonsmooth) eigenfunctions in our numerics (e.g., [31]) and can be suppressed if the resolution is increased further.

solved by expanding each flow variable using the first N Chebyshev polynomials ($N = 300$ is usually sufficient to ensure convergence). An example eigenvalue spectrum for an Oldroyd-B fluid with Wi = 100, $\varepsilon = 10^{-3}$, $\beta = 0.95$, and $k_x = 3$ is reported in Fig. 1 (the bottom right inset shows the equivalent spectrum with $\varepsilon = 0$). The continuous spectra in the absence of polymeric diffusion are regularized with the introduction of $\varepsilon \neq 0$ [30], with a pair of linear instabilities emerging with wavespeeds $c_r \sim \pm 1$.

We map out the unstable region for various parameters and boundary conditions in Fig. 2(a). In the top left panel of Fig. 2(a) we observe that the instability persists as $\varepsilon \to 0$, i.e., this is a singular limit for all three boundary conditions and occurs at a constant value of Wi for diffusivities $\varepsilon \leqslant 10^{-2}$, requiring an increasingly large streamwise wave number $k_x \propto \varepsilon^{-1/2}/8$ (the authors of [30] did not consider these large wave numbers and so failed to find instability). The imaginary part of the wavespeed scales with the square root of the diffusivity $c_i \propto \varepsilon^{1/2}$, so that the growth rate of the instability $k_x c_i$ remains $O(1)$ as $\varepsilon \to 0$. The unstable region appears unbounded as Wi $\to \infty$ for boundary conditions (i) and (ii), but stability is restored in this limit for (iii). Henceforth boundary condition (i) is used.

In Figs. 2(b) and 2(c) we also examine the effect of the viscosity ratio and finite extensibility on the diffusive instability. The instability is realized for decreasing values of Wi at fixed ε as β is reduced (i.e., increasing polymer concentration), and the marginal stability curves collapse when plotted against $\mathrm{Wi}(1-\beta)/\beta$ in the ultradilute limit $\beta \to 1$, which is the magnitude of the perturbation stresses τ'_{xx} and τ'_{xy} relative to the diffusion terms in the momentum equation. Furthermore, the instability survives for realistic values of the polymer extensibility of $L_{\max} = O(100)$, in the FENE-P model, though it is pushed to increasingly low values of β and suppressed beyond a critical Wi. Figure 2(c) shows that this instability is also present in plane Poiseuille flow driven by a non-dimensional pressure gradient $\partial_x P = -2$, the neutral curves nearly overlapping when

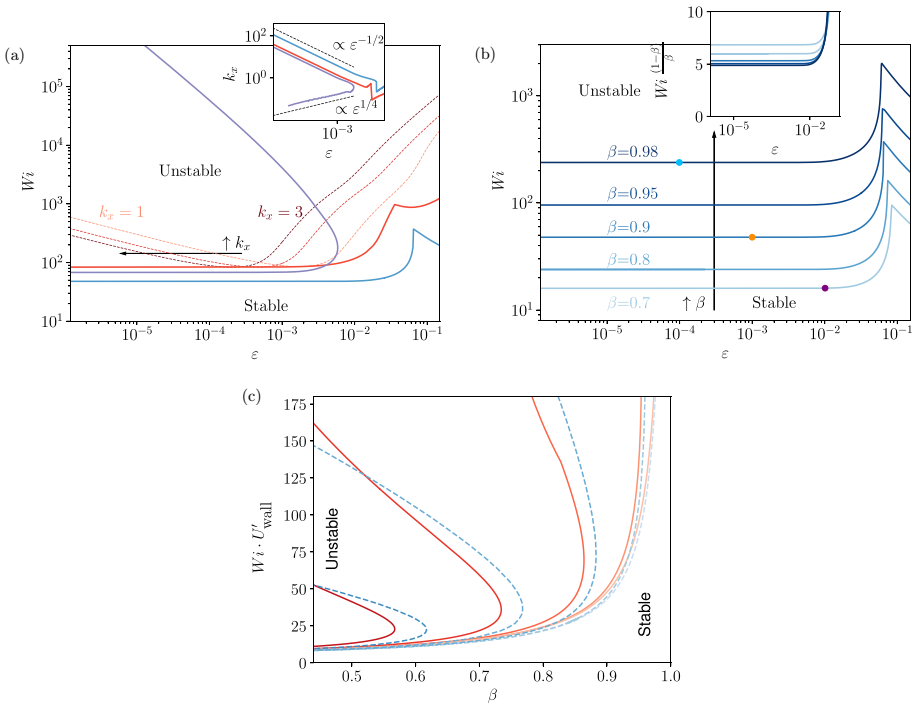

FIG. 2. (a) Neutral curves for Oldroyd-B in the ε-Wi space for $\beta = 0.9$ with different boundary conditions: (i) $\varepsilon = 0$ at the walls (blue); (ii) $\varepsilon \to 0$ only for $\partial_{yy}\mathbf{C}$ (red); and (iii) $\partial_y \mathbf{C} = 0$ (purple). Dashed lines show the neutral curves for individual wave numbers $\{1, 2, 3\}$ with b.c. (ii) Inset shows the wave number k_x along the neutral curves and its scaling with $\varepsilon^{-1/2}$ for all boundary conditions. (b) Neutral curves in the ε-Wi for different β in Oldroyd-B. Inset: collapse of the curves in the ultra-dilute limit $\beta \to 1$, $\text{Wi} \to \infty$. (c) Effect of the adding finite extensibility to plane Couette flow (red solid lines) and plane Poiseuille flow (blue dashed lines) in the FENE-P model. Curves show different values of $L_{\max} = \{\infty, 600, 200, 100, 60\}$, curves from right (lighter shade) to left (darker shade) for $\varepsilon = 10^{-3}$.

Wi is rescaled by the shear rate at the wall, U'_{wall}. The quantitative differences observed between the two flow configurations for the specific case considered in Fig. 2(c) arise due to the relatively large value of $\varepsilon = 10^{-3}$ (the boundary layer has thickness $\varepsilon^{1/2}$), so that the instability is affected by the nonmonotonic channel profile. A neutral eigenfunction is shown in Fig. 3(a), where we visualize contours of the perturbation trace of the polymer conformation and streamlines for an example set of parameters $\text{Wi} = 47.84$, $\beta = 0.9$, $\varepsilon = 10^{-3}$. The spanwise vorticity is shown below in Fig. 3(b) for various values of ε, β, and Wi. The mechanism of instability is reminiscent of the destabilizing effect of viscosity in Newtonian channel flow which subtly adjusts the relative phases of key dynamical processes [32]. In the polymer diffusive instability perturbations to the polymer field are highly stretched in a boundary layer of size $O(\varepsilon^{1/2})$ at one of the walls where the perturbation vorticity is concentrated. Without stress diffusion, the phase of the ensuing polymer stress is poorly matched to that of the velocity field so there is not enough positive feedback in the momentum equation. A diffusive phase lag in the polymer stretch response, however, allows the polymer stress to sufficiently reinforce the flow which created it, thereby producing an instability (see the Supplemental Material for a more detailed description) [42].

The instability described here is realized for commonly used parameters in numerical simulations of dilute polymer solutions (e.g., $\text{Wi} \sim 50$ at $\beta = 0.9$) over a wide range of realistic diffusivities. For example, in a microfluidic context, ε can range from $O(10^{-6})$ for long polymer molecules formed by random chains with contour length much larger than the persistence length to

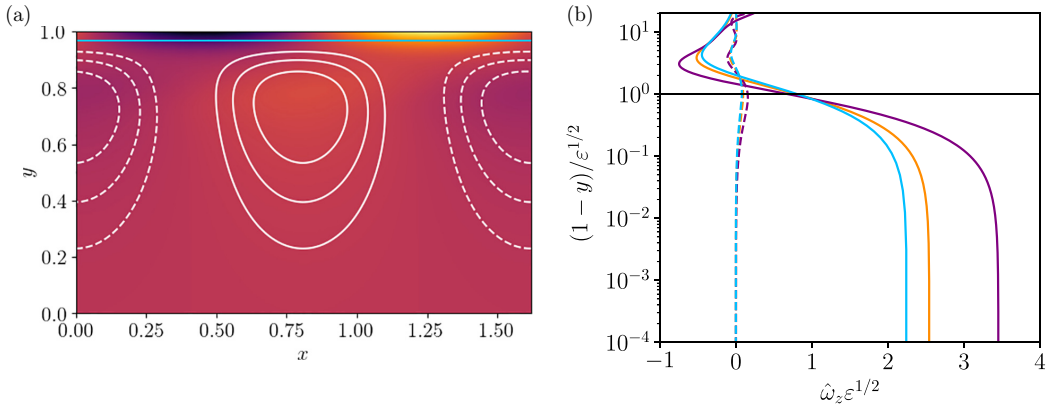

FIG. 3. (a) Pseudocolor corresponding to tr(**C**) of the upper wall eigenfunctions on the neutral curves for the orange point indicated in Fig. 2(b). Contour lines indicate the stream function (flow left to right). (b) Spanwise vorticity for the corresponding coloured dots in Fig. 2(b). The eigenfunctions are normalized so that $\|v_{\max}\| = 1$.

$O(10^{-3})$ for short polymers. The instability exists in a boundary layer of size $\approx 10\sqrt{\varepsilon}$ [see Fig. 3(b)] and has an optimal wave number $k_x \approx 0.125/\sqrt{\varepsilon}$ consistent with this [see Fig. 1(a) in Supplemental Material [42]). Dimensionally, this is a lengthscale of $10\sqrt{\varepsilon}\,h = 10R/\sqrt{\mathrm{Wi}}\sqrt{k_B T\lambda/6\pi\mu_s R^3}$ using the Stokes-Einstein relation ($k_B T$ is the thermal energy and R is the polymer gyration radius) and with typical values (e.g., see [33]) reduces to $\approx 10R/\sqrt{\mathrm{Wi}}$ consistent with the simple scaling relationship $D \sim R^2/\lambda$. The optimal instability lengthscale therefore approaches the polymer lengthscale for $\mathrm{Wi} \gtrsim 100$ although larger-scale instability modes, which offer a better scale separation, also exist away from the neutral curve [see Fig. 1(b) in the Supplemental Material [42]).

We now show, by using the FENE-P model, that this instability forms a pathway to chaos in plane Couette flow. The nonlinear evolution of the diffusive instability is examined by first conducting two-dimensional DNS of the governing equations (1) using the open-source codebase DEDALUS [34]. We perform calculations at parameter settings $\mathrm{Wi} = 100$, $\beta = 0.9$, $L_{\max} = 600$, and $\varepsilon = 10^{-3}$ in a box of length $L_x = 2\pi$ with resolution $[N_x, N_y] = [128, 256]$. The simulations are initialized with low-amplitude white noise, which excites the most unstable mode $k_x = 3$. The unstable mode amplifies exponentially before saturating onto a limit cycle with period $T \sim h/U_0$. We report a snapshot of the instantaneous polymer stretch field in Fig. 4(a) alongside the volume-averaged—denoted $\langle\cdot\rangle$—vertical velocity squared in Fig. 4(b). While the polymer is significantly stretched relative to the laminar value, the velocity fluctuations are relatively low amplitude, $v = O(10^{-2}U_0)$.

In flows with inertia, EIT can be realized in purely two-dimensional configurations [35], which is not something we observe in our inertia-less calculations. The stability of the limit cycle is examined in a three-dimensional configuration with spanwise width $L_z = 2\pi$ by adding small-amplitude white noise in the velocity component w. Three-dimensional simulations were performed with resolutions ranging from $[N_x, N_y, N_z] = [64, 128, 32]$ to $[128, 256, 64]$ to check robustness. A time series of the volume-averaged polymer trace from this computation is reported in Fig. 4(d), which shows a departure from the simple time-periodic solution to a chaotic trajectory which is maintained for over a $10^4 h/U_0$ time period. We believe this to be a numerical realization of elastic turbulence in parallel flow.

An instantaneous snapshot of the chaotic flow can be seen in Fig. 4(c). The horizontal pseudocolor plane located at $y = -0.99h$ (in the boundary layer at the lower wall for $\varepsilon = 10^{-3}$) shows how tr(**C**) is modulated in the both the streamwise and spanwise direction forming high and low high stretch regions. The vertical back plane contours the vertical velocity v, which is amplified in small-scale near-wall patches reminiscent of suction and ejection events in high Reynolds number

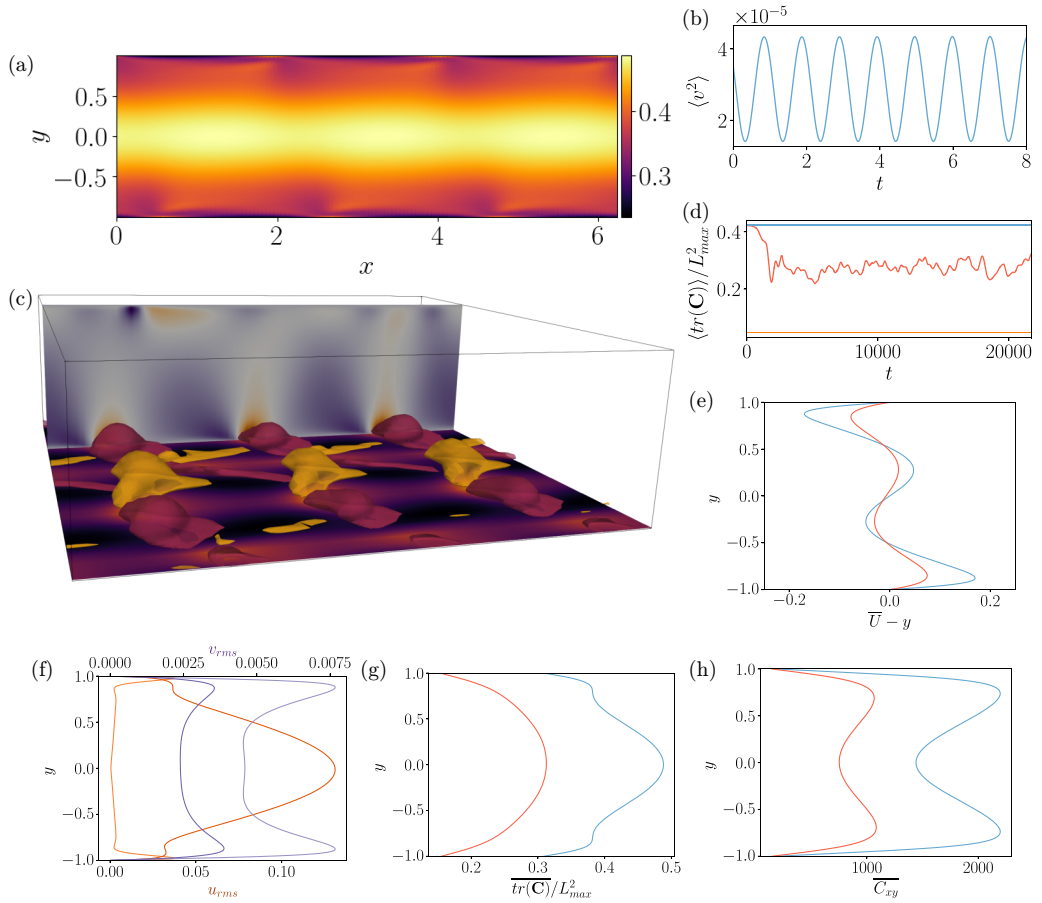

FIG. 4. Direct numerical simulations of inertialess viscoelastic plane Couette flow for Wi $= 100$, $\beta = 0.9$, $L_{\max} = 600$, $\varepsilon = 10^{-3}$. (a) Instantaneous visualization of $\langle \mathrm{tr}(\mathbf{C}) \rangle$ of the two-dimensional periodic orbit identified. (c) Instantaneous visualization of the chaotic three-dimensional state identified. The horizontal slice is a pseudocoulor of $\mathrm{tr}(\mathbf{C})$ at $y = -0.99$, the vertical slice is a pseudocolor of vertical velocity v. The contours indicate positive and negative values of the spanwise velocity w. Flow from left to right. (b) Time series of $\langle v^2 \rangle$ for the two-dimensional nonlinearly saturated state corresponding to a low-amplitude high-frequency periodic orbit. (d) Time series of the volume average $\mathrm{tr}(\mathbf{C})$ for the chaotic three-dimensional flow with the parameters above (red), the two-dimensional nonlinearly saturated state (blue), and the laminar state (orange). (e)–(g) and (h) Time average mean quantities—denoted $(\cdot)$—for the two-dimensional (2D) limit cycle and the three-dimensional (3D) chaotic state; (e) deviation of the mean velocity from $U = y$ (2D blue, 3D red). (f) u_{rms} (purple: 2D light, 3D dark) and v_{rms} (orange: 2D light, 3D dark); (g) $\overline{\mathrm{tr}(\mathbf{C})}/L_{\max}$ (2D blue, 3D red). (h) $\overline{C_{xy}}$ (2D blue, 3D red).

wall-bounded turbulence. The three-dimensional contours (in the box) represent w, illustrating the spanwise motion of the flow.

The statistics of both the limit cycle and the three-dimensional chaotic attractor are examined further in Figs. 4(e) to 4(h), which indicates (i) that the limit cycle is a significant departure from the laminar base state, (ii) the chaos departs from the limit cycle while retaining certain features, and (iii) the polymer is substantially stretched in the center of the domain for both the limit cycle and in the chaotic flow. There are also sharp variations of u_{rms} in a boundary layer $\delta \propto \varepsilon^{1/2}$ at the walls

(verified in computations at various ε but not shown). The values of $u_{\rm rms}$ in ET are significantly different from the limit cycle and reach their largest magnitude at the centerline.

The presence of polymeric stress diffusivity is commonly disregarded in the linear stability analyses of viscoelastic flows [10,11,13,14,36,37]. However, we found that its presence, even at vanishingly small values in the FENE-P model, fundamentally changes the stability of viscoelastic plane Couette flow in the absence of inertia (i.e., vanishing polymer stress diffusion is a singular limit). This polymer diffusive instability (PDI) is a "wall" mode, traveling with roughly the wall speed, and has a streamwise wavelength comparable to the boundary layer thickness. This last feature could easily have led to the instability being dismissed in the past as a numerical instability. The onset of instability is found at Wi ≈ 8 independently of $L_{\rm max}$ and ε for a broad range of β. DNS of the instability leads to a stable periodic orbit in two dimensions and to spatiotemporal chaos in three dimensions, the first numerical realization of such a flow state in a wall-bounded parallel flow configuration. This chaotic state is reproducible in other viscoelastic shear flows with and without inertia [38].

The fact that the PDI operates on a scale approaching the polymer gyration radius at higher Wi ($\gtrsim$100) brings into question whether (i) FENE-P remains a good viscoelastic model there and (ii) whether this instability could be experimentally observed. Certainly at lower Wi $= O(10)$ and for less optimal (larger-scale) PDI modes, there should be sufficient scale separation for the continuum approximation. The bigger issue is whether FENE-P with polymer stress diffusion incorporates enough physics to be realistic when the PDI drives the dynamics. Preliminary calculations in the two-fluid model of [39] (simplified to a solution of Hookean dumbells [40,41], see Supplemental Material [42]) suggest that the added presence of polymer concentration diffusion stabilizes the PDI. This would suggest that the PDI will be not be seen in the laboratory. If that is the case, our results then call into question the continuing use of the FENE-P model which can only be numerically integrated forward in time if polymer stress diffusion is present (either artificially or numerically).

The authors gratefully acknowledge the support of EPSRC through Grant No. EP/V027247/1. The authors declare no competition of interest.

[1] R. Bird, R. Curtiss, R. Armstrong, and O. Hassager, *Dynamics of Polymeric Liquids: Fluid Mechanics*, Vol. 1, 2nd ed. (Wiley, New York, 1987).
[2] A. Groisman and V. Steinberg, Efficient mixing at low Reynolds numbers using polymer additives, Nature (London) **410**, 905 (2001).
[3] T. M. Squires and S. R. Quake, Microfluidics: Fluid physics at the nanoliter scale, Rev. Mod. Phys. **77**, 977 (2005).
[4] E. S. G. Shaqfeh, Purely elastic instabilities in viscometric flows, Annu. Rev. Fluid Mech. **28**, 129 (1996).
[5] A. Groisman and V. Steinberg, Elastic turbulence in a polymer solution flow, Nature (London) **405**, 53 (2000).
[6] R. G. Larson, Turbulence without inertia, Nature (London) **405**, 27 (2000).
[7] A. Groisman and V. Steinberg, Elastic turbulence in curvilinear flows of polymer solutions, New J. Phys. **6**, 29 (2004).
[8] V. Steinberg, Elastic turbulence: An experimental view on inertialess random flow, Annu. Rev. Fluid Mech. **53**, 27 (2021).
[9] P. Pakdel and G. H. McKinley, Elastic instability and curved streamlines, Phys. Rev. Lett. **77**, 2459 (1996).
[10] L. Pan, A. Morozov, C. Wagner, and P. E. Arratia, Nonlinear elastic instability in channel flows at low Reynolds numbers, Phys. Rev. Lett. **110**, 174502 (2013).
[11] R. van Buel and H. Stark, Characterizing elastic turbulence in the three-dimensional von Kármán swirling flow using the Oldroyd-B model, Phys. Fluids **34**, 043112 (2022).

[12] S. S. Datta, A. M. Ardekani, P. E. Arratia, A. N. Beris, I. Bischofberger, G. H. McKinley, J. G. Eggers, J. E. López-Aguilar, S. M. Fielding, A. Frishman *et al.*, Perspectives on viscoelastic flow instabilities and elastic turbulence, Phys. Rev. Fluids **7**, 080701 (2022).
[13] P. Garg, I. Chaudhary, M. Khalid, V. Shankar, and G. Subramanian, Viscoelastic pipe flow is linearly unstable, Phys. Rev. Lett. **121**, 024502 (2018).
[14] M. Khalid, I. Chaudhary, P. Garg, V. Shankar, and G. Subramanian, The centre-mode instability of viscoelastic plane Poiseuille flow, J. Fluid Mech. **915**, A43 (2021).
[15] M. Khalid, V. Shankar, and G. Subramanian, Continuous pathway between the elasto-inertial and elastic turbulent states in viscoelastic channel flow, Phys. Rev. Lett. **127**, 134502 (2021).
[16] J. Page, Y. Dubief, and R. R. Kerswell, Exact traveling wave solutions in viscoelastic channel flow, Phys. Rev. Lett. **125**, 154501 (2020).
[17] Y. Dubief, J. Page, R. R. Kerswell, V. E. Terrapon, and V. Steinberg, First coherent structure in elasto-inertial turbulence, Phys. Rev. Fluids **7**, 073301 (2022).
[18] A. Morozov, Coherent structures in plane channel flow of dilute polymer solutions with vanishing inertia, Phys. Rev. Lett. **129**, 017801 (2022).
[19] G. Buza, M. Beneitez, J. Page, and R. R. Kerswell, Finite-amplitude elastic waves in viscoelastic channel flow from large to zero Reynolds number, J. Fluid Mech. **951**, A3 (2022).
[20] G. H. Choueiri, J. M. Lopez, A. Varshney, S. Sankar, and B. Hof, Experimental observation of the origin and structure of elastoinertial turbulence, Proc. Natl. Acad. Sci. **118**, e2102350118 (2021).
[21] S. Berti, A. Bistagnino, G. Boffetta, A. Celani, and S. Musacchio, Two-dimensional elastic turbulence, Phys. Rev. E **77**, 055306(R) (2008).
[22] S. Berti and G. Boffetta, Elastic waves and transition to elastic turbulence in a two-dimensional viscoelastic kolmogorov flow, Phys. Rev. E **82**, 036314 (2010).
[23] G. Boffetta, A. Celani, A. Mazzino, A. Puliafito, and M. Vergassola, The viscoelastic kolmogorov flow: Eddy viscosity and linear stability, J. Fluid Mech. **523**, 161 (1999).
[24] A. Bistagnino, G. Boffetta, A. Celani, A. Mazzino, A. Puliafito, and M. Vergassola, Nonlinear dynamics of the viscoelastic Kolmogorov flow, J. Fluid Mech. **590**, 61 (2007).
[25] Y. Dubief, C. M. White, E. S. G. Shaqfeh, and V. E. Terrapon, Polymer maximum drag reduction: A unique transitional state, in *Annual Research Briefs* (Stanford, Center for Turbulence Research, 2010), pp. 395–404.
[26] B. Hof, D. Samanta, and C. Wagner, The maximum drag reduction asymptote, Abstract presented at APS Division of Fluid Dynamics, Baltimore, Abstract M8-005 (2011).
[27] D. Samanta, Y. Dubief, M. Holzner, C. Schafer, A. N. Morozov, C. Wagner, and B. Hof, Elasto-inertial turbulence, Proc. Natl. Acad. Sci. **110**, 10557 (2013).
[28] A. W. El-Kareh and L. G. Leal, Existence of solutions for all Deborah numbers for a non-Newtonian model modified to include diffusion, J. Non-Newtonian Fluid Mech. **33**, 257 (1989).
[29] R. Sureshkumar, A. N. Beris, and R. A. Handler, Direct numerical simulation of the turbulent channel flow of a polymer solution, Phys. Fluids **9**, 743 (1997).
[30] P. Chokshi and V. Kumaran, Stability of the plane shear flow of dilute polymeric solutions, Phys. Fluids **21**, 014109 (2009).
[31] H. J. Wilson, M. Renardy, and Y. Renardy, Structure of the spectrum in zero reynolds number shear flow of the ucm and oldroyd-b liquids, J. Non-Newtonian Fluid Mech. **80**, 251 (1999).
[32] C.-C. Lin, *The Theory of Hydrodynamic Stability* (Cambridge University Press, Cambridge, England, 1955).
[33] N. Burshtein, K. Zografos, A. Q. Shen, R. J. Poole, and S. J. Haward, Inertioelastic flow instability at a stagnation point, Phys. Rev. X **7**, 041039 (2017).
[34] K. J. Burns, G. M. Vasil, J. S. Oishi, D. Lecoanet, and B. P. Brown, Dedalus: A flexible framework for numerical simulations with spectral methods, Phys. Rev. Res. **2**, 023068 (2020).
[35] S. Sid, V. E. Terrapon, and Y. Dubief, Two-dimensional dynamics of elasto-inertial turbulence and its role in polymer drag reduction, Phys. Rev. Fluids **3**, 011301(R) (2018).
[36] R. G. Larson, E. S. Shaqfeh, and S. J. Muller, A purely elastic instability in Taylor–Couette flow, J. Fluid Mech. **218**, 573 (1990).

[37] H. A. C. Sanchez, M. R. Jovanovic, S. Kumar, A. Morozov, V. Shankar, G. Subramanian, and H. J. Wilson, Understanding viscoelastic flow instabilities: Oldroyd-B and beyond, J. Non-Newtonian Fluid Mech. **302**, 104742 (2022).

[38] M. M. P. Couchman, M. Beneitez, J. Page, and R. R. Kerswell, Inertial enhancement of the polymer diffusive instability, arXiv:2308.14879.

[39] V. G. Mavrantzas and A. N. Beris, Modeling of the rheology and flow-induced concentration changes in polymer solutions, Phys. Rev. Lett. **69**, 273 (1992).

[40] A. Beris and V. G. Mavrantzas, On the compatibility between various macroscopic formalisms for the concentration and flow of dilute polymer solutions, J. Rheology **38**, 1235 (1994).

[41] W. B. Black and M. D. Graham, Slip, concentration fluctuations, and flow instability in sheared polymer solutions, Macromolecules **34**, 5731 (2001).

[42] See Supplemental Material at http://link.aps.org/supplemental/10.1103/PhysRevFluids.8.L101901 for a more detailed description of this instability.